Beitr. Phys. Atmosph., May 1993, p. 31–43
Article 0005-8173/93/1–2 0031–13 $ 3.00/0 Vol. 66, No.1–2 31

Energy Balance of Solar Power Plants: Results of a One-Dimensional Model

by P. KOEPKE and W. THOMAS*

Meteorologisches Institut der Universität München, Theresienstr. 37, 8000 München 2, Germany

*Now at: DLR, Deutsche Forschungsanstalt für Luft- und Raumfahrt, 8031 Oberpfaffenhofen

(Manuscript received March 11, 1992; accepted April 22, 1993)

Abstract

Installation of solar farms modifies the properties of the surface as boundary between atmosphere and ground. The modified energy balance parameters of the surface are calculated with a one-dimensional stand-alone model. A solar farm with parabolic trough technology is described as a new surface, with an extended energy balance equation containing the terms electrical output and waste heat flux. The resulting changes between a natural surface and the surface "solar farm" are essentially the albedo, which is reduced by about one third of its value, a slightly increased emissivity and a change of surface roughness. On average, 4 % of the incoming solar radiation is transformed into electricity. The sensible heat flux increases significantly, dominantly because of waste heat generated by energy conversion. The calculated variation of the terms of the energy balance allows the estimation of possible climatic effects of solar power plants with extensive mesoscale or general circulation models.

Zusammenfassung

Energiebilanz von Solarkraftwerken: Ergebnisse eines eindimensionalen Modells

Die Installation von Solarkraftwerken verändert die Bodenoberfläche in ihrer Eigenschaft als Grenzfläche zwischen Boden und Atmosphäre. Die dadurch geänderten Energiebilanzterme der Oberfläche werden mit einem eindimensionalen Stand-alone Modell berechnet. Die neue Oberfläche „Solarfarm" wird mit einer um die Terme Elektrizität und Kraftwerksabwärme erweiterten Energiebilanz beschrieben. Wesentliche Änderungen der Eigenschaften bei Wechsel von einer natürlichen Oberfläche zur Oberfläche „Solarfarm" sind eine Reduzierung der Albedo um rund ein Drittel, eine geringe Erhöhung des Emissionsvermögens und eine Änderung der Rauhigkeit. Im Mittel werden 4 % der ankommenden solaren Strahlung in Elektrizität umgewandelt. Der Fluß fühlbarer Wärme ist deutlich erhöht, hauptsächlich aufgrund der Abwärme, die bei der Energieumwandlung freigesetzt wird. Die berechneten Änderungen der Energiebilanzterme erlauben die weitere Untersuchung möglicher Klimaeffekte von Solarkraftwerken mittels aufwendiger mesoskaliger oder globaler Modelle.

1 Introduction

Solar power plants influence the properties of the boundary between the ground and the atmosphere, i.e. the properties of the surface. Therefore, the change of a surface from type "desert" or "savannah" to type "solar power plant" will change its energy balance, with effects on the interaction between surface and atmosphere, and thus possibly influences on local or global climate. These effects should be considered, because the area with solar power plants will increase in the future. For example, in 1989 in the Californian desert regions solar power plants were installed with an electric output of more than 200 Megawatt and an area of 4.5 km^2 (Geyer and Klaiß, 1989). The energy need of the world is estimated to be satisfied by solar power plants with an area of 1 Million km^2.

The climatic effects of large-scale manmade or natural variations of surface properties have been calculated with different models (e.g. Charney et al., 1977; Sud and Fennessy, 1982; Avissar and Verstraete, 1990). However, such models can only be used to detect possible climatic effects of solar power plants if the model relevant properties of a surface formed by a solar farm are known. This information is obtained with the one-dimensional model presented here.

The commercial-scale use of solar radiation is pursued mainly with parabolic trough technology (Klaiß et al., 1987). Consequently, this type of solar power plant is simulated. Such solar power plants consist of receiver field, thermal energy storage medium, heat-engine, turbine and generator. Parabolic receivers focus direct solar radiation on a steel tube surrounded by an evacuated glass tube. Synthetic oil which flows through the steel tube reaches temperatures of up to 400 °C (Harats and Kearney, 1989). This fuel drives a steam-electric generating set and produces electricity. The generated waste heat is delivered into the atmosphere and the cooled oil flows back to the collectors for renewed heating.

The receivers are positioned in rows around the generator building, resulting in the name "solar farm". They are continuously adjusted to an optimum receiver elevation angle relative to the sun by single axis-tracking. The Californian power plants have East-West-facing receivers and a North-South axis of rotation (Geyer and Klaiß, 1989). This type of solar tracking is simulated in the model.

2 Basic Considerations

The goal of this article is to describe a solar farm as a new surface type which results in new lower boundary conditions in the earth-atmosphere system. For this purpose, the vertical extension of the receiver field is assumed to be infinitesimal small in comparison with the height of the atmosphere, in a similar manner to surfaces such as "forest" or "savannah" which consist of many high plants, but are considered to be homogeneous flat surfaces in climate models. Therefore, the bulk properties of a surface "solar farm", that is albedo and emissivity, are calculated, but by modeling a real, vertically structured solar farm.

The used one-dimensional model, called SOFA (SOlar FArm), considers in detail both the horizontal and vertical structure of the receiver field, with vitreous frontside and ceramic backside of receivers and underlying ground and with traffic areas which include buildings. All of the surfaces mentioned have different material properties, i.e. albedo, emissivity, heat conductivity and specific heat, and have different irradiation, because of shadow and tilted receivers. All individual components are assumed to be in thermal equilibrium, so the energy balance of every surface is given as function of its temperature. The model predicts the temperature profiles of air and soil, but uses an external wind, which varies during the day, which, however, is not changed by the solar farm itself. To obtain terms of the energy balance valid for the complete "solar farm", the relevant values for each surface of all the individual components are added, weighted with its relative amount on the whole area of the solar farm and the relevant solid angle (Thomas, 1991).

The energy balance of the surface "solar farm" (Figure 1) is composed of incoming direct, E_s, and diffuse, D, solar and terrestrial, E_t, radiation, the reflected shortwave radiation, M_s, the reflected and emitted thermal radiation, M_t, which together result in net radiation, F_n, and of the latent, L, sensible, H, and soil, B, heat flux. Moreover, the energy balance of the solar farm contains electric output, E_{out}, and the waste heat due to energy conversion, H_e, which is considered as an additional sensible heat flux.

$$F_n + B + H + L + H_e + E_{out} = 0 \qquad (1)$$

The energy balance Eq. (1) describes the solar farm in its entirety, as a new surface type. But each term is calculated under consideration of micrometeorological and radiative processes for all different surfaces of the solar farm weighted with their relative area. All quantities are given as flux densities in Wm^{-2}, and values for the whole "solar farm", especially of interest for the electrical power output, can be calculated by multiplying the given results by the size of the farm.

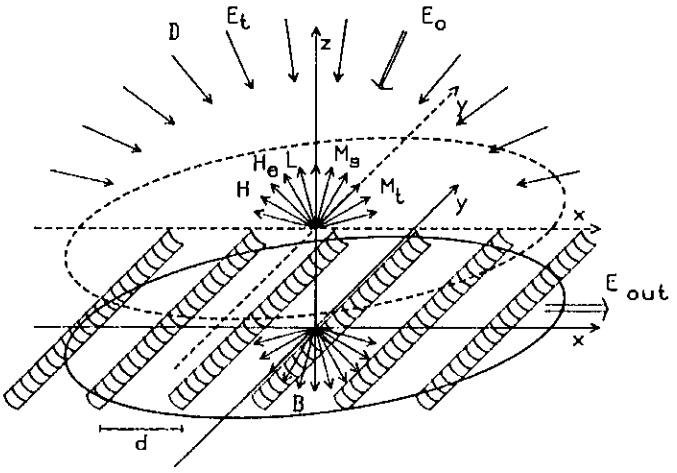

Figure 1 The solar farm, which is considered as a new lower boundary of the system earth-atmosphere with parallel parabolic trough receiver rows with distance d between two rows. The energy balance of the surface "solar farm" is described with shortwave direct, E_s, and diffuse solar radiation, D, longwave atmospheric radiation, E_t, shortwave reflected radiation, M_s, longwave reflected and emitted radiation, M_t, sensible heat flux, H, latent heat flux, L, soil heat flux, B, waste heat flux, H_e, and electrical output, E_{out}.

3 Model

The aim of the model is the simulation of a solar power plant as a surface type. For this purpose, adequately calculated terms of the surface energy balance Eq. (1) are needed and their derivation will be discussed in the next sections. The forcing of the model is the time-dependent shortwave irradiance, which varies in the course of the day due to the change of the sun's position. The model calculates the terms of the energy balance with time steps of five minutes, however, with a time interval of one minute to calculate new temperature profiles of atmosphere and soil.

3.1 Geometrical Considerations

In a cartesian reference frame the solar power plant is placed with rows parallel to the y-axis and receivers rotatable around this axis (Figure 1). The model area is assumed to be periodic in the x-direction, because a collector field consists of many rows with constant distance, d, from one row to the next and with the same orientation of all receiver panels relative to the sun. Additionally, the field is assumed to be homogeneous and infinite in the y-direction, because the rows are much longer than the separation between the rows. Consequently, the receiver field can be described with a one-dimensional, horizontally integrated solution, if the effect of the azimuth angle of the sun is taken into account.

During daytime, the elevation angle of the receiver is optimized so that the incidence angle of the sun is maximum. During night, the receivers are in a horizontal position, but upside down. For a solar farm with North-South oriented receiver rows and with ϑ_0, φ_0 the zenith and azimuth angles of the sun, respectively, the elevation angle of the receiver, ν, is given by Eq. (2), following Stine and Harrigan (1985).

$$\tan \nu = \frac{|\sin \varphi_0|}{\tan \vartheta_0} \tag{2}$$

The effect of direct radiation of the sun is considered by modeling areas under the receivers partly in shadow and in light, and by simulating row-to-row-shading, due to adjacent receiver rows, which all vary with the sun's position during the day.

The diffuse irradiance, both shortwave sky radiation and longwave atmospheric radiation, is modeled by taking into account the parts of the hemisphere shielded by adjacent rows (Figure 2), both for the receivers and for the ground. The following consideration for diffuse radiation is valid, both in solar and terrestrial spectral range, under the assumption of isotropic radiances, I. The resulting irradiance, $F^{\downarrow}$, on an infinite horizontal surface is given by Eq. (3) as the sum of two quarter-spheres with zenith angle ϑ, azimuth angle φ and integration limits, called $f(\psi_i) = \pi/2$, with $i = 1, 2$.

$$F^{\downarrow} = I \left[\int_0^{\pi} \int_0^{f(\psi_1)} \cos\vartheta \sin\vartheta \, d\vartheta \, d\varphi + \int_{\pi}^{2\pi} \int_0^{f(\psi_2)} \cos\vartheta \sin\vartheta \, d\vartheta \, d\varphi \right] \tag{3}$$

In the case of surfaces of the solar power plant, the upper integration limit $f(\psi_i)$ is modified, since the part of the hemisphere which contributes to $F^{\downarrow}$ is reduced by adjacent receiver rows (Figure 2). The perspective effect of an infinite wall, given as elevation angle ψ_i under which the top of the wall is seen, is described with Eq. (4).

$$\tan \psi_i = \tan \Psi_i \cdot \sin \varphi \quad \text{with} \quad i = 1, 2 \tag{4}$$

Here, Ψ_i stands for the maximum elevation angle for perpendicular viewing and φ denotes the azimuth angle, defined with $\varphi = 0$ parallel to the rows, shown in Figure 2 as a wall. The angles Ψ_i depend on the width of the troughs, the height of the pylons, the distance between the rows and time of day, since the receiver inclination is optimized relative to the sun's position.

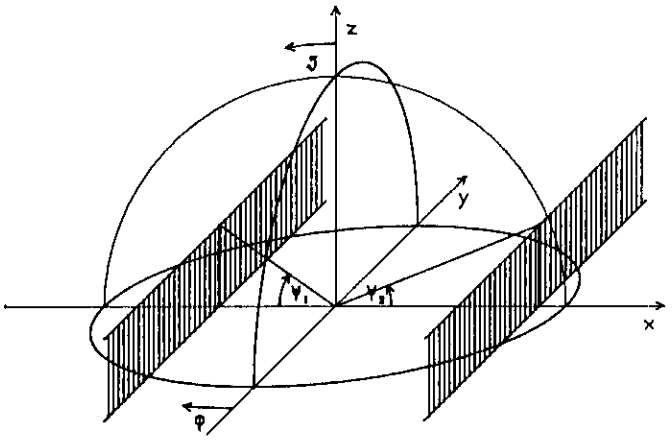

Figure 2 Angles Ψ_1, Ψ_2 used in SOFA to describe geometric limits to simulate the shortwave and longwave diffuse radiation on the surfaces between adjacent parallel receiver rows. See text for details.

The irradiance on a surface between two walls is given by Eq. (3) if the modified integration limits $f(\psi_i) = \pi/2 - \psi_i$ are used, with ψ_i calculated from Eq. (4). The integration is then performed from the zenith down to the top of the adjacent receivers only, taking into consideration the perspective effects. Carrying out the integration over ϑ and φ leads to Eq. (5), which describes the diffuse radiation at a fixed point k between the parallel walls.

$$F_k^{\downarrow} = \frac{I\pi}{2} (\cos \Psi_1(k) + \cos \Psi_2(k)) \quad (5)$$

Thus, the radiation on the two-dimensional surface between the infinite receiver rows is modeled with the one-dimensional Eq. (5), with $\Psi_i(k)$ the only variable beside I. The incoming radiation $F_k^{\downarrow}$ depends on the position of the point k between the two rows. For calculating an average irradiance $\overline{F}^{\downarrow}$, representative for the complete surface between the two rows, Eq. (5) is applied on a number of points, which are equally spaced over d. The arithmetic mean of the results gives $\overline{F}^{\downarrow}$.

Under the made assumption of isotropic radiance distribution, Eq. (5) is also valid for an inclined receiver, if the angles Ψ_1 and Ψ_2 are calculated relative to the tilted surface, or, equivalently, if the zenith angle in Eq. (3) is measured perpendicular to the tilted surface.

Both for the solar and for the terrestrial spectral range, Eq. (5) is used to calculate actual values of diffuse irradiance on front and back of the receivers and on the ground under the receiver rows. As mentioned, the direct radiation on each surface is modeled by taking into account shadows and the actual receiver position. This detailed description is necessary to compute the net radiation, F_n, both for all particular surfaces and for the whole surface "solar farm", with respect to its geometrical properties.

3.2 Shortwave and Longwave Radiation

The time-dependent shortwave global radiation, G, as sum of direct solar radiation, E_s, and diffuse radiation, D, is calculated with an algorithm for cloudfree conditions after Iqbal (1983), which is expanded to allow the simulation of the influence of optically thin cirrus clouds (Koepke et al., 1987). The algorithm takes into account aerosol, water vapour, ozone and gases with constant mixing ratio. The direct radiation is computed as the product of the direct normal solar radiation, E_0, and the cosine of solar zenith angle, θ_0. This procedure is necessary, since only the direct solar radiation is assumed to be concentrated by the receivers to produce electricity. The sun's azimuth and zenith angle are determined as functions of date, time and geographical position of the solar power plant.

Longwave atmospheric radiation at the bottom of the atmosphere, E_t, is calculated as a function of total water vapour content, which is assumed to be constant during the day, and air temperature in a given height, which variation in time is calculated by the model itself. The parameterization in Eq. (6), given by Thiel and Kraus (1986), is applied, which is in good agreement with results from a complex radiative transfer model for an arid summer atmosphere (Mahrer and Pielke, 1977), with $T_a(z_2)$ the air temperature 2 m above ground and e_a the water vapour pressure in hPa. The latter is determined from the total water vapour content already used for calculation of solar radiation, together with climatological values to describe its relation with dewpoint after Smith (1966).

$$E_t = \sigma T_a^4(z_2) \cdot \left(1.0475 - 10^{(-0.424 \cdot (e_a/1.3332)^{0.2})}\right) \quad (6)$$

The temperature $T_a(z_2)$ is derived from the calculated temperature profile (see next section).

3.3 Air Temperature

As mentioned, only the terms of the energy balance of the surface are the goal of this paper. As a consequence, the temperature profile of the atmosphere is needed only to calculate the longwave atmospheric radiation after Eq. (6) and the fluxes of sensible and latent heat of the particular surfaces. The temperature profile $T_a(z)$ from the surface up to the tropopause is calculated by solving a simplified one-dimensional heat transfer Eq. (7) after Zdunkowski et al. (1976), with height dependent turbulent exchange coefficient, $K_h(z)$, after Shir (1973), and the corresponding potential temperature, θ.

$$\frac{\partial \theta}{\partial t} = \frac{\partial}{\partial z}\left(K_h(z) \frac{\partial \theta}{\partial z}\right) \quad (7)$$

In contrast to Zdunkowski et al., the impact of the vertical net flux divergence and the impact of phase change and urban heat sources on the temperature profile are not taken into consideration. In the solar spectral range, water vapour and aerosol are modeled in SOFA with their transmission properties, and the longwave atmospheric radiation at the ground (Eq. (6)) depends on water vapour pressure.

However, an impact of absorption of water vapour and aerosol on net flux divergence and thus on air temperature profile is not taken into account. This effect may lead to heating during daytime and cooling during night-time if strongly absorbing aerosol, like urban aerosol, is present. The magnitude of this effect is small and will be discussed with the results. The influence of phase changes in the atmosphere is assumed to be negligible, since the model is applied only to cloudfree atmospheric conditions in desert regions with low water vapour content. Finally, urban heat sources do not exist. A possible feedback of the generated waste heat of the solar farm (Section 3.9) on the temperature profile is not taken into account, but the consequences again are discussed with the results.

The exchange coefficient in Eq. (7) is used by Shir only for the planetary boundary layer (PBL), however, in our model the PBL is only allowed to vary between 350 m and 3500 m. Hence, the use of the Shir exchange coefficient leads to realistic temperatures, even in the upper troposphere (Thomas, 1991). The lower range limit for the PBL is valid for stable conditions and the upper value is used for unstable conditions.

The upper boundary condition of Eq. (7), $\theta(z_T)$, at the height of the troposphere, z_T, is derived from the temperature of the tropopause and available as function of season and geographical location (Oort and Rasmusson, 1971). The lower boundary condition of Eq. (7) $\theta(z_0)$, at the level of the roughness length, z_0, is calculated after Kleiser (1986), with the potential temperature of the surface, θ_s, the exchange coefficient $K_h(z_{10})$ at the height of the Prandtl-layer, z_{10}, the Karman constant, k, the friction velocity, u_*, and the kinematic viscosity of air, ζ.

$$\theta(z_0) = \theta_s + \frac{K_h(z_{10}) \cdot \frac{\partial\theta}{\partial z}(z_{10})}{k\,u_*} \cdot 0.13 \cdot \left(\frac{z_0 u_*}{\zeta}\right)^{0.45} \tag{8}$$

Eq. (8) relates the potential temperature of the ground beyond and between the receivers, θ_s, to the potential temperature of the lowest layer in the air, by an air flow governed by the local Reynolds number, however approximated to results of laboratory experiments (Zilitinkevich, 1972). Actual and potential surface temperature, $T_g(0)$ and θ_s, respectively, are calculated from thermal equilibrium of the previous time step (see Section 3.4).

Temperature profile and wind profile in the Prandtl-layer are obtained from Eqs. (9) and (10) after Byun (1990), with application of appropriate profile functions (Zdunkowski et al., 1976), Φ_h and Φ_m, of heat and momentum, respectively.

$$\frac{\partial\theta}{\partial z} = \frac{T_*}{kz} \cdot \Phi_h\left(\frac{z}{L_*}\right) \tag{9}$$

$$\frac{\partial u}{\partial z} = \frac{u_*}{kz} \cdot \Phi_m\left(\frac{z}{L_*}\right) \tag{10}$$

T_*, u_* and L_* denote temperature scale, friction velocity and Monin Obukhov length in the surface layer as usual (e.g. Stull, 1988). T_* is obtained from the sensible heat flux at the top of the surface layer (at z = 10 m) by Eq. (11):

$$u_* T_* = K_h(z_{10}) \frac{\partial\theta}{\partial z}(z_{10}) \tag{11}$$

where K_h and θ are given from the boundary layer model (Eq. (7)) as described before.

The friction velocity u_* is obtained by integrating Eq. (10) with windspeed $u(z_{10})$ prescribed as external parameter. From integration of Eq. (9) by using Eq. (11) an effective heat transfer coefficient for the atmospheric surface layer, α_L, can be defined by

$$\alpha_L = \frac{\rho_a c_p T_* u_*}{\theta(z_{10}) - \theta(z_0)} \tag{12}$$

which will be used for evaluation of the latent heat flux in Eq. (15) (Section 3.5), with ρ_a the density of air and $\theta(z_0)$ from Eq. (8).

A water vapour profile is not simulated in our model, because, as mentioned above, water vapour in SOFA is used only to affect the incoming solar and terrestrial radiation (Section 3.2).

The values of the stability parameter (z/L_*) are fixed to the range limits, $-2 \le (z/L_*) \le 1$, which omits unrealistic values of u_* for strongly unstable and strongly stable conditions, respectively. The roughness length z_0 has been chosen as $z_0 = 0.1$ m for the surface "solar farm" (see Section 5.3).

Starting with values L_*, $K_h(z)$, θ_s, $T_a(z)$ from the previous time step, the new profile functions Φ_h, Φ_m and the friction velocity u_* are calculated for the actual time step. With these values, the new profile of the exchange coefficient, $K_h(z)$, and subsequently the temperature profile, $T_a(z)$, with

its actual lower boundary condition, $\theta(z_0)$, are computed.

3.4 Soil Heat Flux

The variation of the temperature profile of the ground, $T_g(-z)$, is calculated with a one-dimensional heat transfer Eq. (13) with the heat conductivity, λ_s, the specific heat, c_s, and the density of the soil, ρ_s, which are assumed to be constant with depth. Soil water is neglected, which is a good approximation since the model is applied for desert regions only. The differential equation is solved with Dirichlet boundary conditions, employing the implicit "Crank-Nicolson-scheme" (Roache, 1982). The upper boundary condition, $T_g(z = 0)$, is the average temperature of the ground beyond and between the receivers, partly in shadow and in light, and calculated from thermal equilibrium of each of the mentioned surfaces. The lower boundary condition, the temperature in depth of 2 m, $T_g(z_g)$, is assumed to be the average annual temperature of the geographic region simulated. The soil heat flux, B, for such a dry and spatially homogeneous ground is calculated by Eq. (14), with Δz the thickness of the first layer of the temperature profile in the soil.

$$\frac{\partial T_g}{\partial t} = \frac{\lambda_s}{\rho_s c_s} \frac{\partial^2 T_g}{\partial z^2} \tag{13}$$

$$B = -\frac{\lambda_s}{\Delta z}\left(T_g(0) - T_g(\Delta z)\right) \tag{14}$$

3.5 Latent Heat Flux

The model is used only for cloudfree conditions, and therefore phase changes of water vapour in the air, and consequently clouds and rain are not taken into consideration. However, SOFA is able to simulate dew on its individual surfaces and the condensed water may be evaporated again if the temperature rises. These processes have influence on the temperature of the particular surfaces. The impact on the temperature profile of the atmosphere is modeled only via the variation of the surface temperature θ_s in Eq. (8), as already mentioned in Section 3.3. Other evaporational processes beside dew are not considered. This is in good agreement with natural surfaces in desert regions and with the collector panels, which have dry interiors. Thus, since only dew can evaporate, Eq. (15) is used to calculate latent heat flux, which is valid for potential evaporation. All particular surfaces used in the model are described with their temperature, T, their temperature-dependent specific heat of evaporation, r (T), actual pressure, p, and saturation vapour pressure, e_s. The heat transfer coefficient for tilted receiver panels is calculated after Thiel and Kraus (1986) and the heat transfer coefficient for the atmospheric surface layer is computed from Eq. (12).

$$L = -\frac{0.622\, r(T)}{p\, c_p}\, \alpha_L (e_s - e_a) \tag{15}$$

The mean evaporation of the total surface "solar farm" is modeled by adding evaporation of every surface, weighted with its relative amount to the whole area of the solar farm.

3.6 Net Radiation

The net radiation, F_n, as the difference between incoming and outgoing shortwave and longwave radiation, is calculated for each of the particular surfaces (receivers and ground beyond and between the receivers) using Eq. (16).

$$\begin{aligned} F_n &= (1 - \rho)\, G + \varepsilon\, (E_t - \sigma T^4) = \\ &= G - M_s + E_t - M_t \end{aligned} \tag{16}$$

G and E_t are the downward shortwave global radiation and the longwave atmospheric radiation, respectively, M_s and M_t are the upward shortwave and longwave radiation fluxes (see Figure 1), and T is the temperature of the particular surface. Incoming and outgoing radiation fluxes are weighted with the angle-dependent influences of the adjacent receivers which are discussed in detail in Section 3.1. For the particular surfaces of the system, both albedo ρ and emissivity ε are material constants.

Eq. (16) is also used to calculate the net radiation of the surface "solar farm". However, in this case the quantities albedo and emissivity describe the entire system "solar farm" and result from the radiative processes at all components of the solar farm as shown in the next section.

3.7 Albedo and Emissivity

The albedo is the ratio of upward shortwave radiation flux, M_s, to downward global irradiance, G.

$$\rho = \frac{M_s}{G} \tag{17}$$

For the "solar farm", the mean reflected radiation, M_s, is calculated via weighted adding of the radia-

tion reflected to hemisphere from each individual surface. This value, and consequently the albedo, which is one of the properties of the new surface "solar farm", depends on solar elevation and azimuth angle and consequently, on geographic position of the solar farm and on time and season. Moreover, the albedo depends on the atmospheric turbidity, which affects the partition of direct radiation and diffuse sky radiation to global radiation. The direct radiation dominantly is absorbed for power generation, hence the reflected radiation is more strongly varied than the incoming global radiation. The simple method to calculate the mean albedo of the "solar farm" by weighting the albedo values of each particular surface with its relative amount, would give unrealistic results.

The emissivity of the surface "solar farm" is calculated in a similar manner. All components of the solar farm receive time-dependent terrestrial radiation (Eq. (6)), which is again coupled with season and geographic position of the solar power plant. The incoming longwave radiation is reflected from each of the particular surfaces, as function of its emissivity, its relative amount on the whole area and on its solid angle subtended by each component, by which the upward hemisphere is seen, which depends on the receiver elevation angle. To obtain only reflected atmospheric radiation, the thermal radiation emitted from every surface is numerically ignored. In this case, the longwave reflectivity of the "solar farm", r_t, is calculated as the ratio of reflected terrestrial radiation, M_r, to downward atmospheric radiation, E_t, and the corresponding emissivity of the system, ε, is calculated by Eq. (18) using Kirchhoffs radiation law:

$$\varepsilon = 1 - r_t = 1 - \frac{M_r}{E_t} \tag{18}$$

The mean temperature of the surface "solar farm" T_{SF}, is determined as a mixture of temperature of the ground under and between the receivers, temperature of the traffic area and different temperatures of both receiver sides, taking into account the different emissivity of the particular surfaces. With calculated values of atmospheric radiation E_t from Eq. (6), emissivity ε after Eq. (18) and upward longwave radiation flux, M_t, which includes both reflected and emitted thermal radiation of all surfaces, the temperature T_{SF} is given by:

$$T_{SF} = \sqrt[4]{\frac{M_t - (1-\varepsilon)\,E_t}{\varepsilon\,\sigma}} = \sqrt[4]{\frac{M_t - M_r}{\varepsilon\,\sigma}} \tag{19}$$

Substituting T in Eq. (16) by T_{SF} leads to the net radiation of the solar farm in its entirety.

3.8 Electric Output

The mean electrical output of the solar power plant, E_{out}, is calculated in Eq. (20) as the product of the direct normal solar radiation, E_0, at the bottom of the atmosphere, with so called optical efficiency, η_o, thermal efficiency, η_t, efficiency of energy conversion, η_c, and the ratio of the total receiver area to the total area of the solar farm, A_r, which is in the order of 0.3 (Geyer and Klaiß, 1989). The electrical output is removed from the system, the energy is no longer available, neither for the ground nor for the atmosphere.

$$E_{out} = -\eta_o\,\eta_t\,\eta_c\,A_r\,E_0 \tag{20}$$

The optical efficiency is calculated taking into account the different losses of radiation on its way from incoming solar radiation to the thermal storage medium. Losses are caused by single-axis tracking, which mostly does not allow perpendicular irradiation, and are caused by row-to-row-shading. Additionally, single-axis tracking systems are affected with loss at the end of the receiver rows, where the incoming radiation cannot be focused on the absorbing steel pipe (Kalt, 1985). Imperfect reflectivity and transmissivity of the mirror, possibly caused by dust, reduces the radiation which is available for absorption. The radiation passes through the vitreous part of the receiver and any dust layer twice, hence the transmissivity of dust layer and mirror is squared, causing reduced values of η_o. However, dust influence is assumed to be small, with a transmission of 0.98, since in practice the mirrors are washed regularly.

Thermal losses of the oil pipes occur on the way from solar field to power block, as described by the according efficiency, η_t.

Energy conversion losses, with η_c for the corresponding efficiency, are dominantly determined by turbine efficiency, but gain in electrical energy is also reduced by consumption on the solar farm itself.

Of course, each of the dimensionless efficiencies are less than 1, with thermal efficiency $\eta_t \approx 0.7$ and energy conversion efficiency $\eta_c \approx 0.27$, averaged over 24 hours, which values are taken from literature (Kalt, 1985). The optical efficiency, η_o, strongly varies with solar position and atmospheric absorbers and scatterers and is calculated by the model itself.

3.9 Waste Heat Flux

All losses due to thermal energy conversion are combined in one additional term in the energy balance equation, the waste heat of the solar farm, H_e. The losses are calculated by one minus the heat related efficiencies, multiplied by direct normal solar radiation, weighted with optical efficiency, and the ratio of the receiver area to the solar farm area (Eq. (21)). It is necessary to take into account the optical efficiency, because only this weighted part of radiation reaches the absorbing elements and is converted to electricity and waste heat.

$$H_e = -(1 - \eta_t \eta_c)\, \eta_o\, A_r\, E_0 \qquad (21)$$

The waste heat flux is assumed to be sensible heat given back to the atmosphere, homogeneously distributed over the solar farm area. As mentioned in Section 3.3, the temperature profile of the atmosphere is not affected by the waste heat.

3.10 Sensible Heat Flux

The sensible heat fluxes of all particular surfaces used in the model, i.e. the ground beyond and between the receiver rows, traffic areas and both receiver sides, are calculated under the assumption of individual thermal equilibrium of each of the mentioned surfaces by using Eq. (1), of course without electric output, E_{out}, and waste heat flux, H_e.

The sensible heat flux of the entire "solar farm", H, however, is considered as a residual term of the energy balance Eq. (1), because weighted adding of the sensible heat fluxes of all particular surfaces would lead to wrong results. Hence, the sensible heat flux is determined using Eq. (22), where all terms have been obtained as area weighted averages of all individual surfaces of the solar farm.

$$H = -(F_n + B + L + H_e + E_{out}) \qquad (22)$$

4 Verification

4.1 Basic Model

The developed model is verified first with respect to meteorological aspects. Therefore, the diurnal cycle of the energy balance of a natural surface, without solar farm, is calculated. For comparison, observed data were used, obtained during a field campaign in the Saharan desert in February 1971 (Tetzlaff, 1974). Hourly data of global irradiance, reflected global irradiance, atmospheric radiation, reflected atmospheric radiation, thermal radiation from the ground, surface heat flux, surface temperature and air temperature in several layers are available. The model was initialized with data, typical for desert regions, i.e. an atmosphere with low moisture content and turbidity and a dry, sandy surface, but without receiver field. The diurnal cycle of wind speed at 5.7 m height is taken from Tetzlaff (1974). Global and atmospheric radiation with its reflected counterparts, and the surface, sensible, and latent heat fluxes are calculated. The latent heat flux is however zero, because minimum temperatures are too high to permit condensation. The diurnal cycles of these measured data are compared with the observed terms of the energy balance.

Figure 3 shows the observed and calculated daily variation of net radiation, F_n, and soil heat flux, B, from 24.2.71 8^{oo} to 25.2.71 13^{oo}. The sensible heat flux, H, is also shown in the figure for completeness although this contains no additional information about the model quality, because the sensible heat flux both in model and in observation is only determined as a residual term of the energy balance. The difference between observed and calculated net radiation is explained by considering its constituent terms. Since no actual information on aerosol amount and properties is available, an appropriate aerosol type (desert dust) is taken from the literature (d'Almeida et al., 1991), with an optical depth which gives the best agreement between observed and calculated global radiation. These data sets fit completely, not shown in a figure, during the whole time considered (Thomas, 1991). The agreement between observed reflected radiation and that calculated with SOFA is also very good. However,

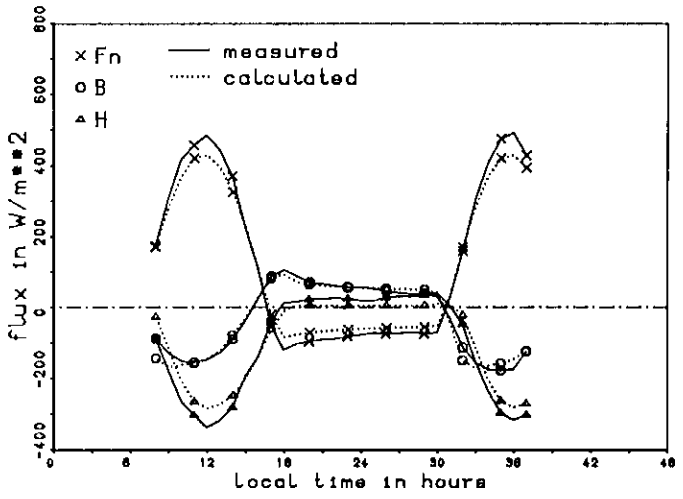

Figure 3 Comparison of net radiation, F_n, soil heat flux, B, and sensible heat flux, H, measured by Tetzlaff (1974) (solid lines) at Saharan desert and calculated with SOFA (dotted lines). See text for details.

the albedo is modeled with a fixed value and does not vary with solar position like the observed albedo. Thus, small differences exist near sunset and sunrise, which do not exceed 10 Wm^{-2}. Consequently, the difference in net radiation shown in Figure 3 is a difference in longwave net radiation, which is maximum around noon with a deviation of $-60\ Wm^{-2}$, or 15 %. The diurnal cycle of air temperature, not shown here, has less variability in the values modeled with SOFA than in the observed ones (Thomas, 1991). At noon, the calculated air temperature is about 3 K less than the observed one and during the night, the modeled air temperature is 3 K higher. This deviation between measured and calculated temperature cycles is also described by Cautenet et al. (1992) and may be explained as a consequence of the neglected impact of net flux divergence on the temperature profile. During daytime, the absorption of "mineral" or "dust-like" aerosol (d'Almeida et al., 1991), leads to higher air temperature (Carlson and Benjamin, 1980) and during the night, lower air temperature is regarded, because the upward longwave radiation increases due to higher emissivity of the desert aerosol. Additionally, advective effects are not taken into consideration in SOFA, but may influence the observed quantities.

The computed soil heat flux corresponds well with observed values. Differences of more than 10 Wm^{-2} only occur at the beginning of the simulation and in maximum values on the second day. In addition to this deviation, the maximum values of the second computed day show a phase lag, resulting from an increase of surface temperature towards the end of the measuring period.

The deviation from computed to observed diurnal cycles of air temperature and the terms of energy balance, which on average is in the order of 10 %, is also found by Cautenet et al. (1992). We are therefore confident, that the simple one-dimensional model "SOFA" is of relatively high accuracy, with all relevant atmospheric processes included and modeled sufficiently correct.

4.2 Solar Farm

Observations of terms of the energy balance of a solar farm in its entirety are not available. Thus, the quality of the model with respect to the solar farm, with its optical and other technical aspects, is assessed by comparing observed and calculated values of gained electrical output as function of solar irradiance.

The available data set (Geyer and Klaiß, 1989) contains diurnal sums of direct normal irradiance and electrical output of an existing solar power plant with parabolic trough technology, from January to May 1988. The configuration of this solar farm is that used in the model (Thomas, 1991). Atmospheric conditions are chosen with regard to the location in the Californian desert regions, with water vapour after Garrison and Adler (1990), aerosol after d'Almeida et al. (1991), and cirrus conditions after Warren et al. (1986).

Figure 4 shows daily electrical output of the solar power plant, E_{out}, as function of daily direct normal irradiance. For every month, values are calculated for the 1st and 15th day, both for turbid and clear atmosphere, caused by different aerosol amount. Five values per month, representative for the whole month, are taken from measured data.

The simulated values agree well within the range of variation of the observed ones. In January, the difference between observation and simulation has its maximum. The calculated electrical output is too high, because of the data which are used to model the efficiency of energy conversion. This value is available only for a mean summer day (Kalt, 1985), but in wintertime the capacity of a solar farm is not fully used and consequently, the efficiency of energy conversion is reduced.

This verification shows that the aspects of receiver positioning and reflection properties are modeled correctly. We are therefore confident, that the model, with its detailed description of energy balance at each of the different surfaces, is adequate

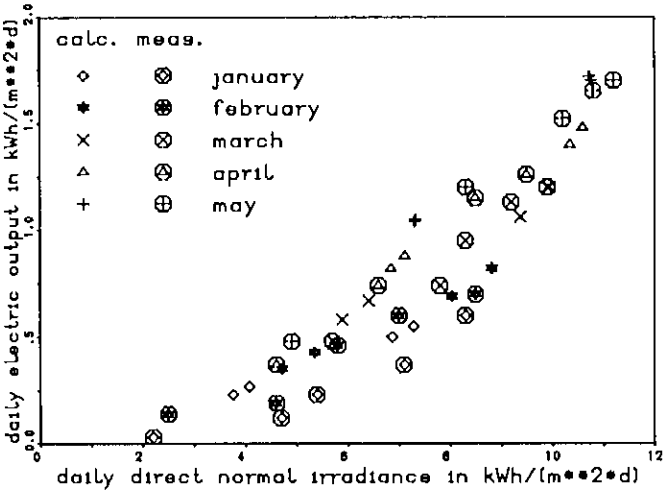

Figure 4 Comparison of data of mean daily values of direct normal solar irradiance and resulting electric output for January to May, measured (symbols with circle) at the solar power plants in California (Geyer and Klaiß, 1989) and calculated (symbols without circle) with SOFA.

for the determination of properties of the new surface "solar farm".

5 Results

5.1 Energy Balance of Solar Farm

Calculated diurnal cycles of all the terms in the energy balance of a solar farm (Eq. (1)) are shown in Figure 5. Since solar power plants in particular exist in the Californian Mojave desert, this geography is simulated, with corresponding atmospheric conditions. To simulate an average summer day, the orbit of the sun valid for the 1st May is used. The properties of the particular components of the solar farm are chosen so as to model the solar power plants in California (Geyer and Klaiß, 1989) and are described in detail by Thomas (1991).

Electrical output, E_{out}, is about 4 % of the incoming radiation, in the solar spectral range, a value typical for solar power plants. Net radiation of the system, F_n, is balanced mainly by sensible heat, H, and waste heat, H_e, from the power station, which is about four times the electrical energy, due to the low efficiency. With the modeled daily and nocturnal thermal conditions of a desert summer atmosphere, condensation and evaporation are not possible, thus, L is calculated to be zero. The soil heat flux, B, reaches a maximum value in the early morning, and decreases linearly during the day. This is a result of receiver shadow on the ground, which prevents the maximum of soil heat flux later in the morning, typical for a desert surface.

As mentioned, the simple model used neglects flux divergence due to absorbing aerosol and water vapour, and consequently, the atmospheric longwave radiation has too low values during daytime. Additionally, the waste heat of the solar farm, which is given back to the atmosphere as latent heat, is not taken into account to increase the air temperature. On the other hand, the thermal losses even of the oil pipes are modeled as latent heat. The pipes are isolated but warmer than the receivers and the ground and this leads to a mean temperature of the solar farm which is higher than calculated. These effects can be estimated to balance each other, so the radiation balance modeled for a solar farm is better than supposed from Figure 3.

5.2 Energy Balance Alteration by a Solar Farm

The change of the energy balance of a surface as a consequence of the installation of a solar farm is examined by simulating both a natural surface and, with identical external conditions, the new surface "solar farm". The geographic location, date of simulation and mean atmospheric conditions are the same as used for calculation shown in Figure 5. All terms shown in Figures 6 and 7 as function of time are differences. A positive difference indicates that the corresponding value has increased according to the installation of the solar farm, negative difference denotes a decreased value. The signs of the terms in the energy balance must, however, be considered. During the daytime, the surface and sensible heat fluxes are negative. Hence, if the flux

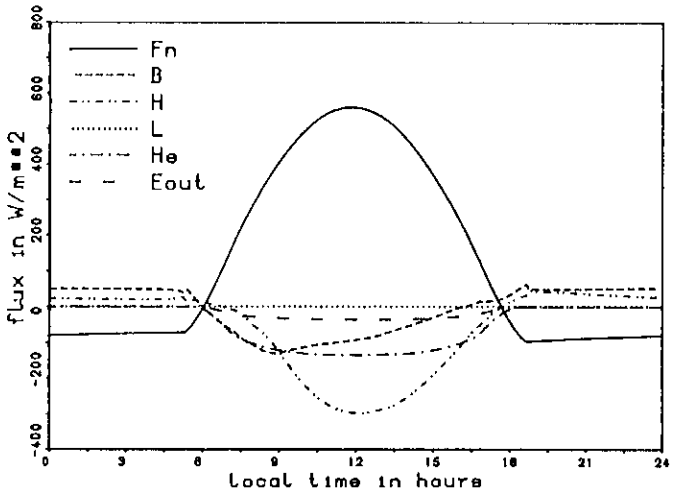

Figure 5 Energy balance of a surface "solar farm", calculated with SOFA for the properties of solar power plants in California for 1st May (Geyer and Klaiß, 1989), with net radiation, F_n, soil heat flux, B, sensible heat flux, H, latent heat flux, L, waste heat flux, H_e, and electric output, E_{out}.

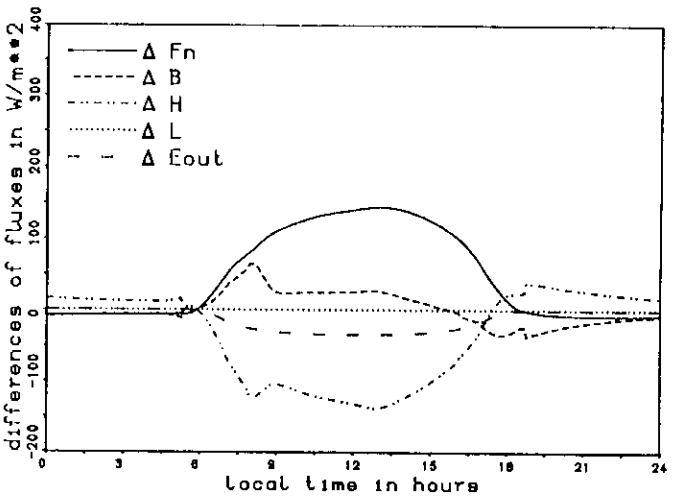

Figure 6 Differences of terms of energy balance, calculated by a change from surface "desert" to surface "solar farm", with differences of net radiation, ΔF_n, soil heat flux, ΔB, sensible heat flux including waste heat, ΔH, latent heat flux, ΔL, and electric output, ΔE_{out}.

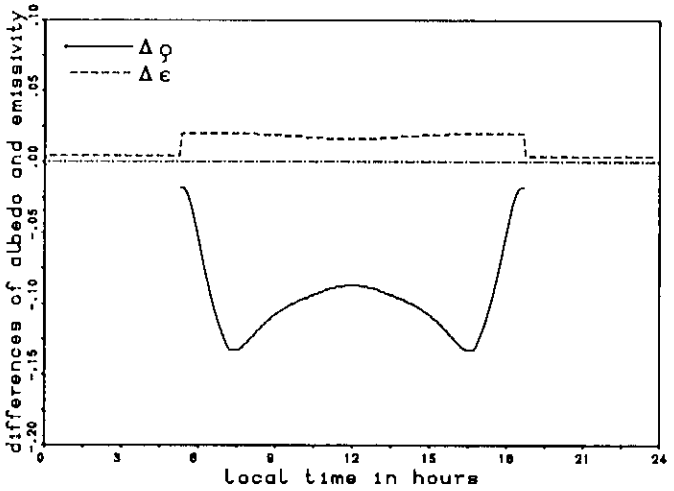

Figure 7 Differences of albedo, Δρ, and emissivity, Δε, calculated by a change from surface "desert" to surface "solar farm".

increases in the case of "solar farm" the differences are negative and vice versa.

Figure 6 shows the change of the terms of energy balance in case of "solar farm", compared to that without. Reflected solar and emitted thermal radiation are reduced in case of solar farm, and therefore the difference in net radiation, ΔF_n, is increased. In the shortwave spectral range radiation from the sun is absorbed for energy conversion and not available for reflection. The upward radiation flux in the longwave part of spectrum is also decreased during the day, because the shadows reduce the temperature of the ground beyond the receivers. During the night, the thermal radiation in the case of "solar farm" is slightly increased, because horizontally positioned receiver panels absorb incoming atmospheric radiation. Therefore, at the ground under the receivers, atmospheric radiation is replaced by thermal radiation from the collectors, which is larger, since their temperature is close to the air temperature. During the day, shadow cast by the receivers leads to decreased surface temperature. Hence, the soil heat flux is reduced, with a positive difference in soil heat flux, ΔB, together with a reduced sensible heat flux from the ground and from the receivers. However, the latter effect is more than compensated by the waste heat from energy conversion. This is taken into account as additional sensible heat and included in the difference in sensible heat flux, ΔH, shown in Figure 6. This combination of higher sensible heat flux and lower surface temperature is the most unexpected effect resulting from the installation of a solar farm. Under the simulated thermal conditions, neither condensation nor evaporation occurs. Thus, the latent heat flux is equal to zero in both simulations and, consequently, so is the difference, ΔL. The difference in electricity, ΔE_{out}, of course, is increased in the case of "solar farm", as it was zero without the farm.

5.3 Properties of Surface "Solar Farm"

Surfaces in climate models are described by their albedo, ρ, emissivity, ε, and roughness length, z_0. These properties are changed if a solar farm is installed. Moreover, the energy used for electricity production has to be taken into account. The albedo of the surface "solar farm" is reduced, compared to that of the same desert surface without solar farm, due to the solar radiation which is not reflected, but absorbed for energy conversion. Figure 7 shows the albedo difference, Δρ, between the surface "solar farm" and a natural desert with albedo $\rho = 0.38$ (Fischer, 1988). In the simulated case of a farm with North-South oriented rows, the optical efficiency is highest near sunrise and sunset, when the sun's position is East or West. As a consequence, during this time the albedo is reduced most strongly, by about 0.13, that is by one third of its natural value. Around noon, the albedo reduction is lower, on the order of 0.1, since the receivers are horizontally positioned.

The emissivity of the surface "solar farm" is changed both by the properties of the new materials and by the increased surface area, which is able to emit radiation. The emissivity of glass and ceramic is taken with $\varepsilon_g = 0.94$ and $\varepsilon_c = 0.90$, respectively (Kuchling, 1981; d'Ans and Lax, 1967). The latter is lower than that of a sand surface with $\varepsilon_s = 0.93$ (Fischer, 1988), however, the effect of increased emitting surface area dominates, resulting in a slight increase of emissivity, Δε, shown in Figure 7.

The roughness length is not modeled, but estimated from the literature with $z_0 = 0.1$ m. Using an equation from Norman (1990), which allows one to consider the height of the receivers and the distance between the receiver rows, the roughness length is calculated to be $0.05\ \text{m} \le z_0 \le 0.15$ m, with the low values for flat receiver position around noon and during the night. These values are in good agreement with values from Stull (1988) for surfaces "many hedges" with $z_0 = 0.08$ m, and "many trees, hedges and a few buildings" with $z_0 \approx 0.25$ m. In any case, the values for "solar farm" are higher than those proposed for desert or as a North-African average which is $z_0 = 0.003$ m (Stull, 1988).

6 Summary and Conclusion

An extended solar farm is modeled with respect to changed properties of the boundary earth-atmosphere, described as a new surface, called "solar farm". The receiver elements focus direct solar radiation on absorbing heat collection elements and thus reduce the albedo. Only a small part of the absorbed energy is converted to electricity, due to the low efficiency of this process. The dominant part is given back to the atmosphere as waste heat, which enhances the sensible heat flux.

The optical efficiency of a solar farm depends both on the position of the sun and on the ratio of direct to diffuse solar radiation. Hence, it depends on the geographical location, time of year and atmospheric conditions and, consequently, the quantities modeled to describe the surface "solar farm" in its entirety show a certain variability. However, in comparison to the natural surface "desert" or "savannah", the new surface "solar farm" usually will have reduced albedo, slightly changed emissivity and increased roughness length.

Thus, in general a solar farm will act as a heat island. As a consequence, its climatic effects could be opposite to that of increased albedo and reduced roughness length, valid e.g. for deforestation as estimated by Nobre et al. (1991). The results of the simple one-dimensional model SOFA, presented here, allow the investigation of possible climatic effects of solar farms by extensive general circulation models.

Acknowledgements

We thank J. Ackermann and R. Forkel for helpful discussions and we appreciate the critical remarks of our reviewers.

References.

Avissar, R. and *M. M. Verstraete,* 1990: The representation of continental surface processes in atmospheric models, Rev. Geophys., **28**, 35–52.

Byun, D. W., 1990: On the Analytical Solution of Flux-Profile Relationship for the Atmospheric Surface Layer, J. Appl. Met., **29**, 652–657.

Carlson, T. N. and *S. G. Benjamin,* 1980: Radiative Heating Rates for Saharan Dust, J. Atmos. Sci., **37**, 193–213.

Cautenet, G., M. Legrand, S. Cautenet, B. Bonnel and *G. Brogniez,* 1992: Thermal Impact of Saharan Dust over Land. Part I: Simulation, J. Appl. Met., **31**, 166–180.

Charney, J. G., W. J. Quirk, S. H. Chow and *J. Kornfield,* 1977: A comparative study of the effects of albedo change on drought in semi-arid regions, J. Atmos. Sci., **34**, 1366–1385.

d'Almeida, G. A., P. Koepke and *E. Shettle,* 1991: Atmospheric Aerosols. Global Climatology and Radiative Characteristics, A. Deepak Publishing, Hampton, Virginia, 401 pp.

d'Ans, J. and *E. Lax,* 1967: Taschenbuch für Chemiker und Physiker, Band I, 3. Auflage, Springer-Verlag, Berlin, Heidelberg, New York, 751 pp.

Fischer, G., 1988: Landolt-Börnstein, Neue Serie, Gruppe 5, Band 4, Meteorologie, Teilband c, Klimatologie, Teil 1, Springer Verlag, 35 pp.

Garrison, J. D. and *G. P. Adler,* 1990: Estimation of precipitable water over the United States for application to the division of solar radiation into its direct and diffuse components, Sol. Energy, **44**, 225–241.

Geyer, M. and *H. Klaiß,* 1989: 194 MW Solarstrom mit Rinnenkollektoren, BWK, **41**, 288–295.

Harats, Y. and *D. Kearney,* 1989: Advances in Parabolic Trough Technology in the SEGS Plants, presented at: 1989 ASME International Solar Energy Conference, San Diego, April 1989.

Iqbal, M., 1983: An Introduction to Solar Radiation, Academic Press, New York, 175 pp.

Kalt, A. C., 1985: Sonnenenergienutzung durch Parabolrinnenanlagen, BWK, **37**, 488–492.

Klaiß, H., J. Nitsch and *M. Geyer,* 1987: Wirtschaftlichkeitsanalyse von großen Solarkraftwerken, DLR-Nachrichten, **52**, 40–43.

Kleiser, T., 1986: Numerische Simulation von Sekundärzirkulationen in städtischen Bereichen auftrund von Bodeninhomogenitäten, Diplomarbeit für Meteorologie, Karlsruhe, 33 pp.

Koepke, P., H. Quenzel and *R. Sizmann,* 1987: Yearly yield of solar CRS process heat and temperature of reaction, In: Solar Thermal Energy Utilization, Vol. 1, Springer-Verlag, Berlin, Heidelberg, New York, London, Paris, Tokyo, 19 pp.

Kuchling, H., 1981: Taschenbuch der Physik, Verlag Harry Deutsch, Thun und Frankfurt/Main, 579 pp.

Mahrer, Y. and *R. A. Pielke,* 1977: A numerical study of the airflow over irregular terrain, Beitr. Phys. Atmosph., **50**, 89–113.

Nobre, C. A., P. J. Sellers and *J. Shukla,* 1991: Amazonian Deforestation and Regional Climate Change, J. Clim., **4**, 957–988.

Norman, J., 1990: Private communication, University of Wisconsin, Madison, USA.

Oort, A. H. and *E. M. Rasmusson,* 1971: Atmospheric Circulation Statistics, NOAA Professional Paper, **5**, 204 pp.

Roache, P. J., 1982: Computational Fluid Dynamics, Hermosa Publishers, Albuquerque, New Mexiko, 85 pp.

Shir, C. C., 1973: A preliminary numerical study of atmospheric turbulent flows in the idealized planetary boundary layer, J. Atmos. Sci., **30**, 1327–1339.

Smith, W. L., 1966: Note on the Relationship between Total Precipitable Water and Surface Dewpoint, J. Appl. Met., **5**, 726–727.

Stine, W. B. and *R. W. Harrigan,* 1985: Solar Energy Fundamentals and Design, John Wiley & Sons Inc, 61 pp.

Stull, R. B., 1988: An Introduction to Boundary Layer Meteorology, Kluwer Academic Publishers, Dordrecht, Boston, London, 380 pp.

Sud, Y. C. and *M. J. Fennessy,* 1982: A study of the influence of surface albedo on July circulation in semi-arid regions using the GLAS GCM, J. Climatol., **2**, 105–125.

Tetzlaff, G., 1974: Der Wärmehaushalt der zentralen Sahara, Berichte des Instituts für Meteorologie und Klimatologie der Technischen Universität Hannover, **13**, 113 pp.

Thiel, D. and *H. Kraus,* 1986: Solar Flat-Plate Collector Energetics, Beitr. Phys. Atmosph., **59**, 552–572.

Thomas, W., 1991: Energie- und Wärmebilanz von Solarkraftwerken, Diplomarbeit für Meteorologie, München, 158 pp.

Warren, S. G., C. J. Hahn, J. London, R. M. Chervin and *R. L. Jenne,* 1986: Global Distribution of Total Cloud Cover and Cloud Type Amounts over Land, NCAR Technical Note, NCAR/TN-273+STR, DOE/ER/60085-H1.

Zdunkowski, W., R. M. Welch and *J. Pägle,* 1976: One-dimensional Numerical Simulation on the Effects of Air Pollution on the Planetary Boundary Layer, J. Atmos. Sci., **33**, 2399–2414.

Zilitinkevich, S. S., 1972: Boundary Layer in the Atmosphere, In: Parameterization of sub-grid scale processes, Appendix A, GARP Publications Series No. **8**, 7.